Final Draft
of the original manuscript:

Reimann, M.; Goebel, J.; dos Santos, J.F.:

Microstructure and mechanical properties of keyhole repair welds in AA 7075-T651 using refill friction stir spot welding

In: Materials and Design (2017) Elsevier

DOI: 10.1016/j.matdes.2017.07.013

Microstructure and mechanical properties of keyhole repair welds in AA 7075-T651 using refill friction stir spot welding

Authors:

Martin Reimann[a], Jannik Goebel[a], Jorge F. dos Santos[a]

Affiliations:

[a] Helmholtz-Zentrum Geesthacht, Institute of Materials Research, Materials Mechanics, Solid State Joining Processes Department, Max-Planck-Str. 1, 21502 Geesthacht, Germany

Corresponding author:

Martin Reimann. Tel.: +49 4152 872073 fax: +49 4152 2033 mail: martin.reimann@hzg.de

Abstract

To develop a suitable keyhole closure process in high-strength AlZnMg(Cu) alloys, refill friction stir spot welding was used to perform repair welds of through holes of 7.5 mm diameter in AA 7075-T651 plates with 6 mm thickness. The thermal cycle and the evolution of microstructural features were investigated in detail. The mechanical performance of the welds was studied based on the changes in microstructure and temperature exposure caused by the welding process.

Thermal cycle measurements revealed high heating rates and peak temperatures of up to 540°C in the weld center. Leftover grains from the base metal that did not recrystallize were determined in the stirred zone of the weld center. The welds showed a W-shaped hardness distribution with a lowest hardness of 70 % of base metal values in the heat affected zone. Under quasi-static loading, two failure modes were determined, with mode 1 failure occurring in the heat affected zone and mode 2 failure occurring in the outer regions of the stirred zone with crack initiation in the lower portions of the weld. Post-weld natural aging was proven to be highly significant for the mechanical properties of the welds and is effective for up to 4 weeks after welding.

Keywords

Friction spot welding; keyhole closure; termination hole, FSW exit hole, repair weld

1 Introduction

High-strength aluminum alloys are widely used in the transportation industry due to their high strength-to-weight ratio and the increasing need to reduce environmental impact. With advances in technology, the demand has increased for complex products, which must be produced using several processing methods. During processing of aluminum alloys, a wide range of defects can appear, especially during welding operations. Examples include hot cracking and porosity in fusion welds or volume defects of groove, cavity and tunnel in solid-state processes such as friction stir welding. At the end of friction stir welds, the termination hole of the welding tool inevitably remains and reduces the weld strength due to the small joining area. This occurrence is particularly problematic in circumferential welds in which runoff plates are challenging for geometrical and metallurgical reasons. Additional repair applications that lack a satisfactory solution are keyhole closures of drilled-out defects such as damage to keyholes or crack repair. Conventional fusion welding is difficult in the repair process due to an unfavorable distribution of brittle solidification products, cracking, porosity and major strength loss due to high heat input in the weld region, as summarized by Çam and Mistikoglu (2014). Certain alloys, such as the widely used AA 7075, are considered highly complicated to weld with conventional techniques.

The search for a suitable keyhole closure technique that fulfills the requirements for high-quality repair welds has become a research hotspot because friction stir welding and bobbin tool friction stir welding are promising technologies for current space and aircraft manufacturing. Thus, this research focuses on friction-based processes due to encouraging results obtained in the past with these technologies.

In friction taper plug welding (FTPW or friction plug welding, FPW), which is primarily used by The Welding Institute (Dunkerton et al., 1991), a tapered plug is forced co-axially into a keyhole with a similar taper. The conical surface of the plug is friction welded to the surface of the hole. In this method, post-machining is necessary on both sides of the workpiece to remove the unconsumed portions of the plug and the material that is extruded out of the plate. Du et al. (2016) used FPW to seal the through holes in AA 2219-T87 plates with 10 mm thickness and found FPW to be feasible only in tapered and not in standard through holes. The tamper angles of the hole and plug must be compatible to ensure that the typical defects in the lower portions of the weld are extruded out of the plate. The maximum tensile strength of the friction plug welds was 72.3 % of the base metal strength with the thermo-mechanically affected zone located close to the bonding interface, noted as the weakest location of the joints. Metz et al. (2012) applied FPW in friction stir-welded AA 2195-T8 aluminum-copper-lithium alloy plates with 6.36 mm thickness. The major plug diameter was 33 mm, and the minor diameter was 15.9 mm. The weakest area was measured near the plug weld interface, with 65 % of base metal hardness. In a different study, Metz and Barkey (2012) found the strength of the same plug welded samples to be 57 % of the base metal strength compared with 68 % of the BM strength in friction stir-welded samples.

Filling friction stir welding (FFSW), as presented by Huang et al. (2011), is derived from the plug welding process. A shoulder portion is added to the tapered plug to avoid stress concentration at the interface between the plug and hole. Huang et al. (2011) sealed the exit holes with a diameter of 9.8 mm left by FSW using FFSW in Al-Cu-Mg alloy plates with 7.8 mm thickness. Additionally, friction stir processing was used to reprocess the sealed keyholes with a rotating non-consumable tool consisting only of a steel shoulder without a probe. The keyhole closure welds reached a tensile strength of 84.3 % of the base welds conducted by FSW. Han et al. (2013) used the same approach of filling a keyhole left by FSW with FFSW and subsequently using friction stir processing as a post-weld processing step. Han and colleagues used a plug with a diameter of 10 mm made of AA 7075 to seal keyholes in an AA 2219 plate with 7.8 mm thickness and achieved 96.6 % of the FSW base weld strength. Behmand et al. (2015) applied FFSW to remove an exit hole 6.5 mm deep of friction stir welded lap joints in AA 5456. The failure load on the coupons with the refilled keyhole reached 91 % of the corresponding defect-free FSW joint.

Zhang et al. (2014) modified the FFSW method using a pin-free tool and a T-shaped filler bit to reduce the setup time for replacement of the tool between the filling and reprocessing operations. Zhang and colleagues sealed keyholes left by FSW in AA 1060 sheets with 4.7 mm thickness. To eliminate voids in the lower portion of the weld, Zn braze foil was pre-placed in the keyhole. The ultimate tensile strength of the keyhole closure welds achieved 67.3 % of the base metal strength. Until now, FFSW has only been proven to seal keyholes left by a conical FSW tool, for which the geometry of the filler bit must be adapted and has not yet been applied to through holes.

Recently, a method for active-passive filling friction stir repair (A-PFFSR) was introduced by Ji et al. (2016a) in an AZ31-B magnesium alloy. A-PFFSR is a multi-stage process that uses different filler bits and non-consumable pinless tools. First, two active filling steps are applied that reshape the keyhole left by FSW. Finally, passive filling is performed using a disc-shaped filler material. The filling material is heated by frictional heat generated by the pinless tool. Additionally, the forging force created by the tool is beneficial to creating a bond between the filling material and surrounding workpiece. To obtain a sound surface formation, the rotating tool must move transversally along the base friction stir weld after the dwelling period. Later, the same authors applied the technique in 7N01-T4 aluminum alloy sheets with 4 mm thickness (Ji et al., 2016b). A-PFFSR was used to seal keyholes left by the FSW process, reaching 82.1 % of the tensile strength of the FSW base welds and 69.9 % of the base metal tensile strength.

Self-refilling friction stir welding (SRFSW) was proposed by Zhou et al. (2012) to seal the keyhole left by FSW in stainless steel. This multi-stage process uses a series of non-consumable tools with gradual changes in pin geometry and size. A wide and shallow exit hole remains at the surface due to the lack of filler material. SRFSW is not applicable to through holes and, until now, has not been proven to work in aluminum alloys.

Reimann et al. (2016) proposed refill friction stir spot welding (RFSSW) to seal through holes in AA 6061-T6 workpieces. This method seals through holes by applying a plug as filler material and using RFSSW to join the plug to the surrounding workpiece. In plates of AA 6061-T6 with 6 mm thickness, RFSSW-welded

samples reached 68 % and 55 % of the base metal ultimate tensile strength and yield strength, respectively. Later, Reimann et al. (2017) applied RFSSW for termination hole closure in bobbin tool friction stir welds in sheets of AA 2198-T8 with 3 mm thickness. The mechanical performance of the closed holes is similar to the performance of RFSSW keyhole closure welds in the base metal. Efficiencies of 67 % for hardness, 57 % for yield strength and 78 % for ultimate tensile strength were achieved. Keyhole closure using RFSSW was demonstrated as a universal through-hole closure method that offers advantages such as defect-free welds and superior surface appearance on both sides of the weld. Additionally, this method does not require any surface preparation before or after the welding process and seals the keyhole in a single-step process.

Until now, the literature has lacked application studies that seal through holes in high-strength aluminum alloys such as the AlZnMg(Cu) alloy AA 7075 with superior mechanical properties. In its conventional applications, RFSSW was used to weld overlapping sheets of AlZnMg(Cu) alloys, e.g., by Shen et al. (2013) in AA 7075-T6 and Zhao et al. (2014) in alclad 7B04-T74 aluminum alloy. Both studies found the material difficult to weld with defects in the weld zone, such as voids, incomplete refill and lack of mixing, especially at higher plunge depths of more than 2 mm.

RFSSW was proven as a promising method for sealing through holes in precipitation-hardened aluminum alloys with sheet thicknesses up to 6 mm. However, the influence of the process parameters on the mechanical behavior of the welds and the microstructural evolution in the weld zone have not been studied in depth.

In the current work, RFSSW is used to perform repair welds of through holes 7.5 mm in diameter in AA 7075-T651 plates with 6 mm thickness. The thermal cycle and the evolution of microstructural features were investigated in detail. To characterize the repair method, the mechanical performance of the welds was studied based on the changes in microstructure and temperature exposure induced by the welding process. Because AA 7075 is a precipitation-hardened aluminum alloy, the influence of post-weld natural aging on the mechanical properties was analyzed, offering evidence of the importance of this phenomena in 7XXX-series alloys. Additionally, the influence of the process parameters on the mechanical performance and microstructural features was evaluated.

2 Materials and Methods

2.1 Aluminum alloy 7075 – T651

The material used in the current study is a AA 7075-T651 plate with 6 mm thickness. The chemical composition and mechanical properties of this material are listed in Table 1 and Table 2. The plugs used as filler material for keyhole closure are machined from extruded rods made from the same aluminum alloy. The temper used was T651, i.e., solution heat treated, stress relieved by stretching and artificially aged.

Table 1 Chemical composition of the 7075 aluminum alloy used in this study (wt.%)

Al	Cr	Cu	Mg	Mn	Si	Ti	Zn	Fe	Other
89.39	0.19	1.57	2.63	0.05	0.084	0.038	5.82	0.18	0.04

Table 2 Mechanical properties of the AA 7075-T651 used in this study

Hardness (HV0.2)	Yield strength (MPa)	Tensile strength (MPa)	Elongation (%)
184.9	529.3	576.1	14.79

2.2 Experimental procedure

To apply the keyhole closure process, through holes with diameters of 7.5 mm were drilled in the base metal. Cylindrical plugs of the same material and identical dimensions were inserted manually into the holes. The repair welds joining the plug and the surrounding workpiece were performed according to the sleeve plunge process, as reported in (Reimann et al., 2016) and (Reimann et al., 2017) using custom-built equipment designed to investigate the RFSSW process. The RFSSW process uses a non-consumable tool consisting of three independent movable parts, i.e., a clamping ring, a sleeve and a probe, as shown in Figure 1. Threaded RFSSW tools made of molybdenum-vanadium alloyed hot-work tool steel with a clamping ring 17 mm in diameter, a 9 mm sleeve and a 6 mm probe were used. The chosen plunge depth of the sleeve is 5.85 mm to ensure joining of the entire plug to the surrounding workpiece. The actual weld is performed by creating metallic bonding between the material that refills the cavity left by the retracting sleeve during the second phase of the process and the surrounding workpiece. To avoid lack of refill, as reported by Shen et al. (2013) for higher plunge depth, the cavities between the tool parts must be filled with aluminum by plunging into blind base metal with a plunge depth that is significantly higher (7.5 mm in this case) before repair welding. This process impedes material flow into the tool during the actual repair welds. Additionally,

in keyhole closure, this effect can be avoided by the use of a plug with a height slightly larger than the surrounding workpiece.

The welding parameters in this study were rotational speed, plunge speed and retract speed of the sleeve. The rotational speed is similar for the sleeve and probe, and thus, no relative movement exists between them in a rotational sense. The plunge/retract speed of the probe is derived from the speed of the sleeve and front surface ratio of the probe and sleeve. To maintain a constant volume, the cavity underneath the probe must take up the same volume that is pushed away by the plunging sleeve. The probe must retract further than the sleeve plunges because the front surface of the sleeve is larger than that of the probe. Additionally, the influence of dwell time at the highest plunge depth and post-weld natural aging on the mechanical properties was analyzed. The process parameters used in this work are summarized in Table 3. The range of process parameters was developed to produce flawless welds. Welding with process parameter combinations outside of the given window results in flaws such as voids or incomplete refill in the AA 7075-T651 base metal. To analyze the mechanical performance, the process parameters of rotational speed and plunge/retract speed were tested in a 3^3 full factorial design with 9 center point replicates. The revolutions per mm plunge and retract can be calculated using these process parameters, similar to the commonly used weld pitch ratio in friction stir welding. Analysis of dwell time was conducted by holding for 2, 4 and 6 seconds at the maximum plunge depth with 2 replicates each with the center point parameters. The influence of post-weld natural aging was tested by performing hardness and tensile tests at different days of aging up to a maximum of 25 weeks. The thermal cycle was tested using a 3 x 3 matrix with 3 center point replicates. The process parameters used in the thermal cycle analysis were the rotational and plunge/retract speed of the sleeve.

Table 3 Process parameters used in this study

Rotational speed (1/min)	Plunge speed (mm/s)	Retract speed (mm/s)	Dwell time (s)	Post-weld natural aging
1500 – 2100	0,7 - 1	0,7 - 1	2,4 and 6	up to 25 weeks

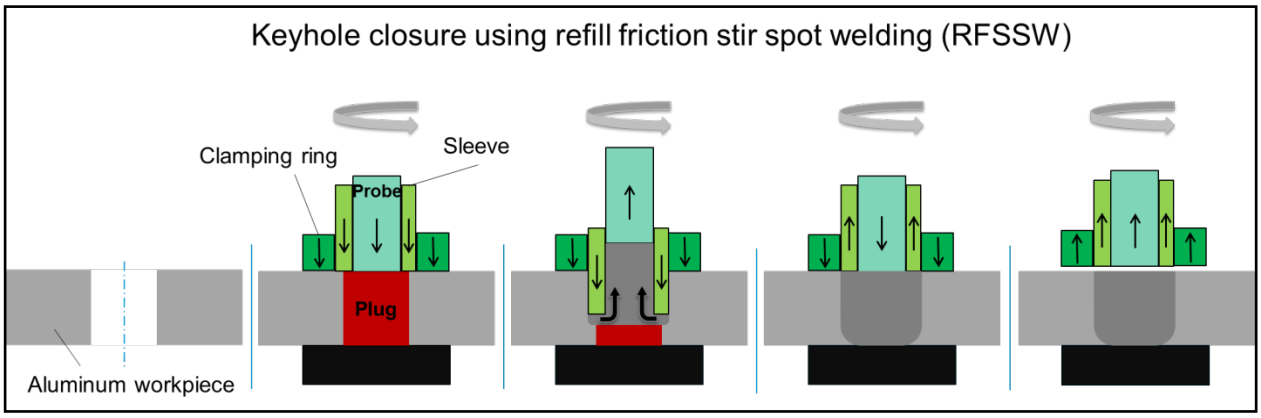

Figure 1 RFSSW keyhole closure process. Initial step: Front surface of rotating tool parts initially contacts the surface of the plate, thus generating frictional heat. Second step: Sleeve plunges downward, displacing material that flows into the cavity underneath the retracting probe. Third step: Probe moves downward and sleeve retracts, pushing softened material back into the weld. Final step: Tool retracts form workpiece, leaving the plug and surrounding workpiece joined. Adapted from (Reimann et al., 2016)

2.3 Analysis and testing techniques

To record the thermal cycle during welding, K-type thermocouples were embedded in the aluminum plates at mid-thickness at a distance of 9 mm and 17 mm from the center of the weld, as shown in Figure 2. Additionally, the thermal cycle in the weld center was measured by applying a thermocouple at a depth of s3 mm from the lower surface for center point measurements. The total energy input was calculated from force and torque measurements, as described by Reimann et al. (2017).

For microstructural analysis, samples were prepared by standard metallographic specimen preparation procedures using flat grinding and finish polishing. For microstructural analysis using polarized light microscopy, samples were anodized using a 3 vol pct solution of HBF4, known as BARKER solution, at 24 V for 2 min. The grain size was measured using LEICA software following ASTM standard E112-13. The cross-sections are never located in the exact center of the circular welds, which changes the size ratios of microstructural features. The correction method for measurements of circular features reported by Reimann et al. (2017) was used to compensate. Additionally, a stop-action method was applied to visualize the material flow and study the microstructure formation. For this purpose, the rotational movement of the tool was stopped as the tool parts were suddenly lifted from the sheet during the process.

The keyhole closure RFSSW process was performed in rectangular coupons, as shown in Figure 2. For mechanical testing, the welded samples were machined to a dog-bone shape with a gauge length of 50 mm. The gauge width was defined as 1.5 times the sleeve diameter, whereas the thickness was given by the thickness of the plate. Other sample dimensions were calculated following DIN 50125:2009-07. Tensile tests were performed in accordance with ISO 6892-1:2009 testing in the rolling direction at a speed of 1 mm/min. The coupons were tested with no further surface or heat treatments. Fracture surface analysis was

performed using a FEI Quanta 650 FEG scanning electron microscope. For optical displacement measurements during tensile testing, a digital image correlation system (ARAMIS, developed by GOM) was used consisting of a CCD camera and a sensor connected to a computer with image elaboration software. The processor was directly connected to the tensile testing machine to obtain each load level related to the acquired images. The hardness measurements were conducted on a Zwick Vickers hardness tester (LECO, type M-400-H) in accordance with ISO 6507-1:2005.

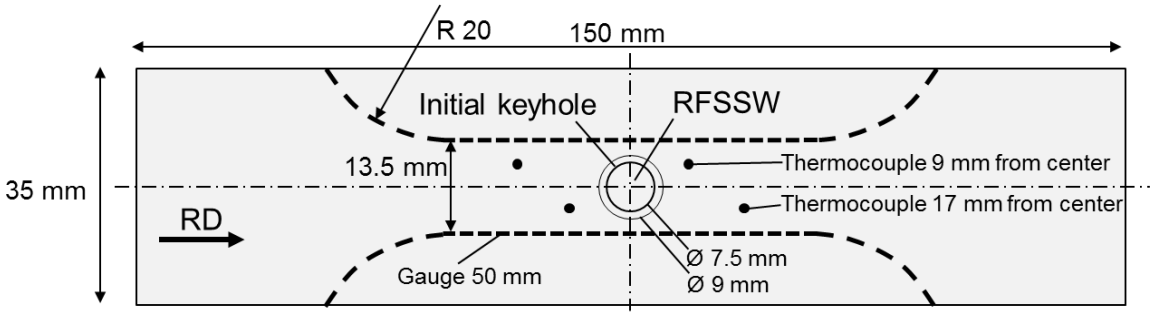

Figure 2 RFSSW welded coupons, adapted from (Reimann et al., 2017)

3 Results

3.1 Thermal cycle analysis

Figure 3 shows a typical thermal cycle during keyhole closure welding at the center point process parameter conditions. The temperature rises during the plunge phase of the sleeve with high heating rates depending on the distance from the center of the weld. In the center of the weld, the peak temperature of 540°C is reached at mid-process when the sleeve arrives at the highest plunge depth. At 9 and 17 mm from the center of the weld, peak temperatures of 368°C and 273°C are reached, respectively, during the sleeve retraction phase. After the welding process, the tool is withdrawn from the surface of the plate, and the temperature is evened out during the cooling process.

Lloyd and Chaturvedi (1982) observed dissolution of all strengthening precipitates above 300°C in AA 7075. Thus, it can be assumed that precipitate dissolution in and around the weld spot is the major strength-reducing mechanism. In the outer areas of the HAZ, over-aging phenomena are assumed to be the leading cause of strength loss.

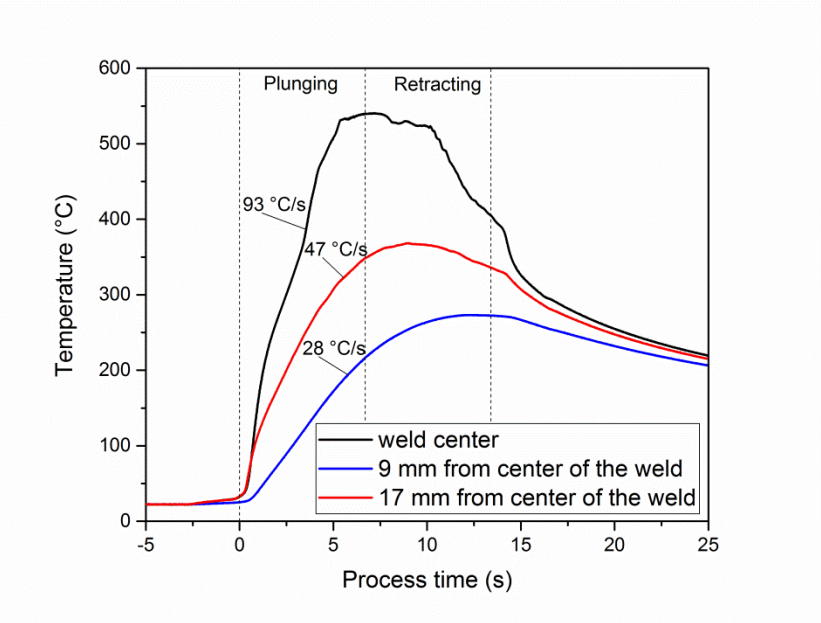

Figure 3 Thermal cycle of keyhole repair weld using RFSSW with 1800 rpm and 0.85 mm/s sleeve plunge and retract speed

An increase in the sleeve revolutions per mm plunge and retract leads to an increase in the supplied energy, as shown in Figure 4. An increase in the revolutions per mm plunge/retract creates an increase in the distance over which the frictional resistance must be overcome at the tool parts in contact with the aluminum. This observation is equivalent to higher energy input. The linear characteristic of the measurements

indicates that the frictional condition between the tool and workpiece does not change significantly in the observed process parameter range.

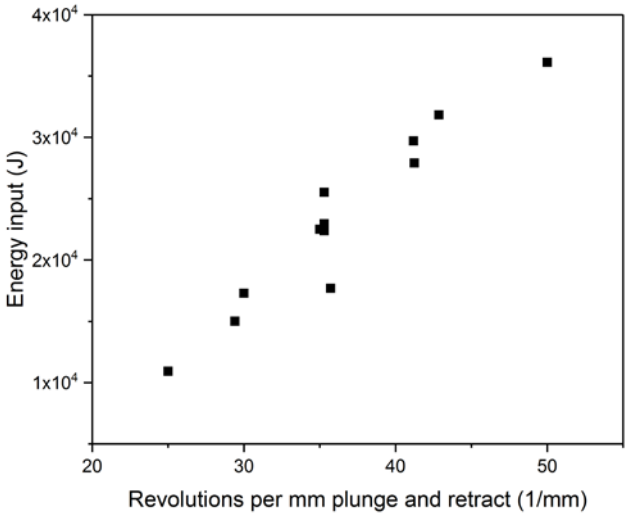

Figure 4 Increase in energy input with increasing sleeve revolutions per mm plunge and retract

Although the energy input is constantly generated over the weld processes with different durations, the peak temperatures in the HAZ are correlated with the supplied energy. A higher energy input increases the peak temperatures in the HAZ, as shown in Figure 5. The increase in energy input from 10 to about 40 kJ causes an increase of approximately 20°C at 9 and 17 mm from the center of the weld. With higher temperatures during the process, the heat dissipation is higher at similar boundary conditions, thus compensating for the higher heat input. This explains the moderate increase in peak temperature when the applied heat is increased significantly.

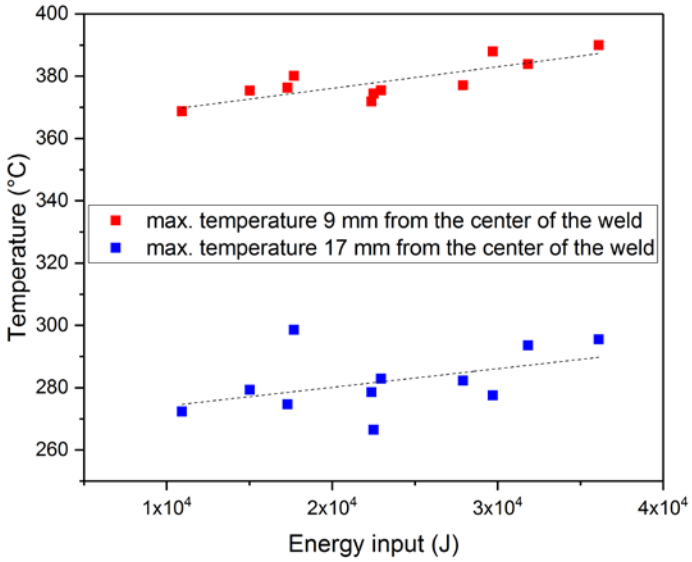

Figure 5 Energy input causes an increase of peak temperatures at locations 9 and 17 mm from the center of the weld

Zhao et al. (2015) performed conventional RFSSW with a sleeve plunge depth of 3 mm in overlapping AA 7B04-T74 sheets with 3.8 mm thickness, similar to AA 7075. At 9 mm from the center of the weld, Zhao and colleagues reported a peak temperature of approximately 280°C with application of 1500 rpm and 1 mm/s plunge/retract speed. Using the same process parameters, the peak temperature was measured as significantly higher, i.e., 386°C, at the same distance from the center of the weld. The higher heat input due to higher plunge depth/longer welding times in combination with presumably similar environmental and heat dissipation conditions causes higher temperatures in the HAZ in this study.

3.2 Microstructure characterization

3.2.1 Microstructural features of keyhole closure welds

The macroscopic structure of a typical cross-section before and after the RFSSW keyhole closure process is shown in Figure 6. In the pre-welded cross-section, the plug made from the extruded rod shows typical elongated grains vertically, whereas the workpiece material shows elongated pancake-shaped grains in the rolling direction.

As shown in Figure 6b), the through hole was successfully re-filled by joining the plug and the surrounding workpiece. Based on the characteristics of the cross-section, the weld structure is found to be symmetrical with respect to the tool axis. The macrograph of the welded sample displays a defect-free microstructure without a lack of refill or voids. The initial interface between the plug and the surrounding workpiece is no longer visible.

The microstructure can be classified into four regions that are typical of friction-based processes in aluminum alloys, i.e., stirred zone (SZ), thermo-mechanically affected zone (TMAZ), heat affected zone (HAZ) and base material (BM). The HAZ undergoes a thermal cycle during the welding process and experiences no plastic deformation. The grain size in the HAZ corresponds to the unaffected base material. The TMAZ is subjected to moderate temperatures and strain rates and is characterized by a deformed microstructure. In the cross-section shown in Figure 6, the grains in the TMAZ are bent upward in the direction of the retracting sleeve. The TMAZ has a torus-like shape that is concavely arched away from the center of the weld with a thickness of approximately 1.4 mm at mid-height. Recrystallization does not occur in the TMAZ due to insufficient deformation strain, which distinguishes the TMAZ from the SZ. In the SZ, both the temperature and strain rates reach their highest values, forcing the microstructure to recrystallize. The SZ is approximately 400 to 600 µm wider than the sleeve diameter, indicating high shear rates and temperatures leading to dynamic recrystallization on the outside of the rotating sleeve.

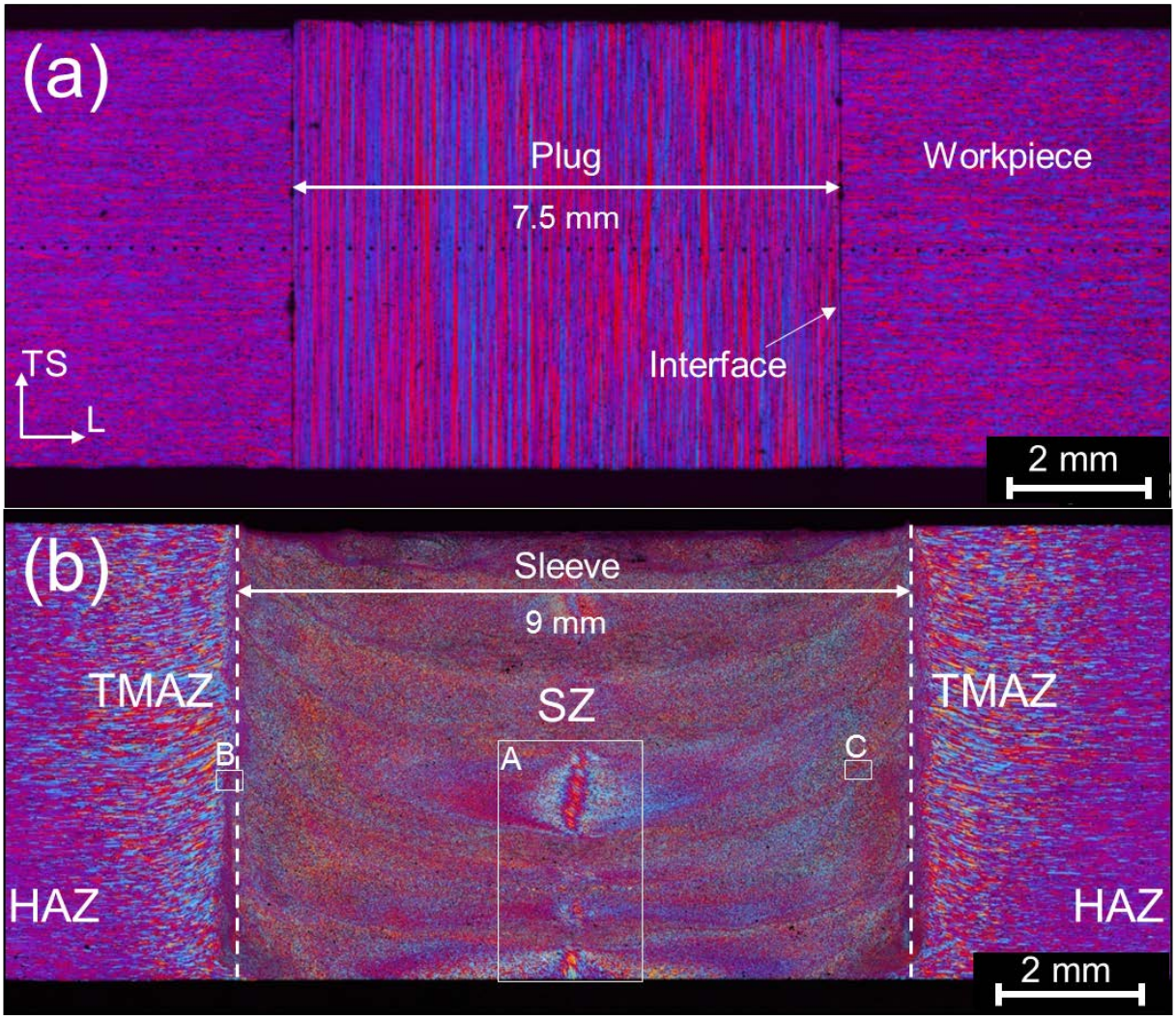

Figure 6 Low-magnification overview of unwelded and welded samples: (a) unwelded cross-section with extruded plug and surrounding workpiece, (b) typical appearance of welded sample

It is the accepted view that the material in the SZ experiences dynamic recrystallization and forms fine equiaxed grains because these features define the SZ. Fine equiaxed grains have been reported in Reimann et al. (2016) and Reimann et al. (2017) for keyhole closure processes using RFSSW in AA 6061-T6 and AA 2198-T8, respectively. For conventional RFSSW in AlZnMg(Cu) alloys, Shen et al. (2013) and Zhao et al. (2015) reported full recrystallization in the stirred zone. Shen et al. (2013) noted a difference in grain size in the SZ and reported much finer recrystallized grains in the outer regions of the SZ than in the center of the weld as well as a variation in the thickness direction. For other friction-based processes in AA 7075, Gerlich et al. (2006) observed fine recrystallized grains in the SZ of the friction stir spot welded microstructure.

Magnified views of regions A, B and C in Figure 6 are shown in Figure 7 to investigate the SZ in detail. Figure 7(A) shows the typical inhomogeneity of the grains in the SZ observed in this study. In the center of

the SZ at the lower portions of the welded plates, deformed grains are visible that are assumed to be leftover grains from the initial microstructure of the plug. The elongated grains of the plug experienced strain rates that are not sufficiently high to recrystallize the material. The grains are deformed due to the shear introduced by rotating tool parts. The grains of the SZ that are fully recrystallized show an average diameter of 4 µm. In the regions of the SZ that surround the diameter of the sleeve, a grain size gradient with decreasing diameter was measured in the direction toward the center of the weld from 5 to 3 µm, as shown in Figure 7(B). The regions of the SZ that were in direct contact with the outer surface of the rotating sleeve exhibit the smallest grains. Additionally, a significant change in grain size is visible in the transition from the SZ to the TMAZ. Figure 7(C) shows a layer of smaller grains approximately 2.5-3 µm in diameter that typically appear in the SZ. These layers are assumed to originate from higher shear during the refilling stage of the process. The layers have a concave shape and are visible throughout the entire SZ. In the center of the weld, the layers are not as defined as in the outer regions, where they are quite sharp with a thickness near 35 µm. The interruption of the un-recrystallized grains in the center of the weld in detail A) are assumed to be caused by these shear bands.

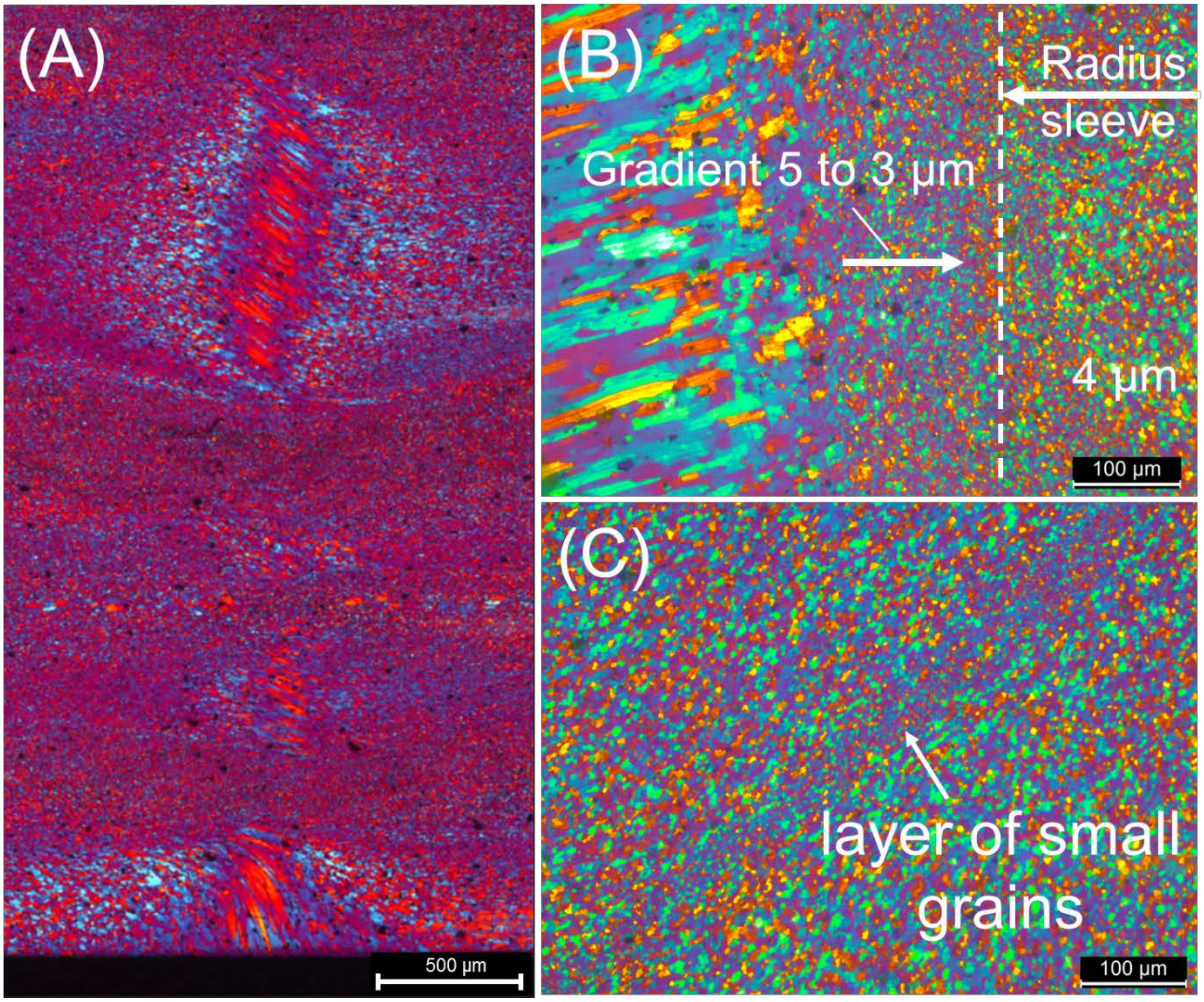

Figure 7 Magnified views of regions A, B and C marked in Figure 6: (A) partial recrystallization and inhomogeneous grain structure in the SZ, (B) grain size gradient in outer portions of the SZ, (C) layer of small grains in the SZ

Cross-sections of the keyhole closure weld location formed via RFSSW in the L-TL plane are shown in Figure 8. Detail (a) reveals circular weld formation at mid-thickness. Figure 8(b) shows elongated grains in the circumferential direction and certain globular grains at approximately 1 mm from the center of the weld. Figure 8(c) reveals fine globular grains only. Thus, fully recrystallized equiaxed grains occur in the outer areas of the SZ only. The fully recrystallized grains in the outer areas are small with diameters of 4 µm. It is unlikely that the elongated grains in detail (b) are formed from recrystallized and grown grains. The elongated grains are assumed to form from not recrystallized base metal.

The multi-phased aluminum alloy used in this study contains coarse intermetallic particles (often referred to as constituent particles) that form during ingot solidification and are too coarse to interfere with the movement of dislocations or grain boundaries. During rolling, these particles fracture, which causes them to become aligned in the rolling direction (Totten and MacKenzie, 2003). In the BM, the constituent particles are found

aligned in the L direction. Figure 8(b) shows alignment of the constituent particles in the circumferential direction in accordance with the grain deformation, but in Figure 8(c), no structure of the particles is apparent.

The transition zone from the SZ to the TMAZ is shown in Figure 8(d). In the rotational direction, deformed grains are revealed in the beginning of the TMAZ. These grains appear to be of medium size and without a defined structure in the L-TS cross-section in Figure 7(b).

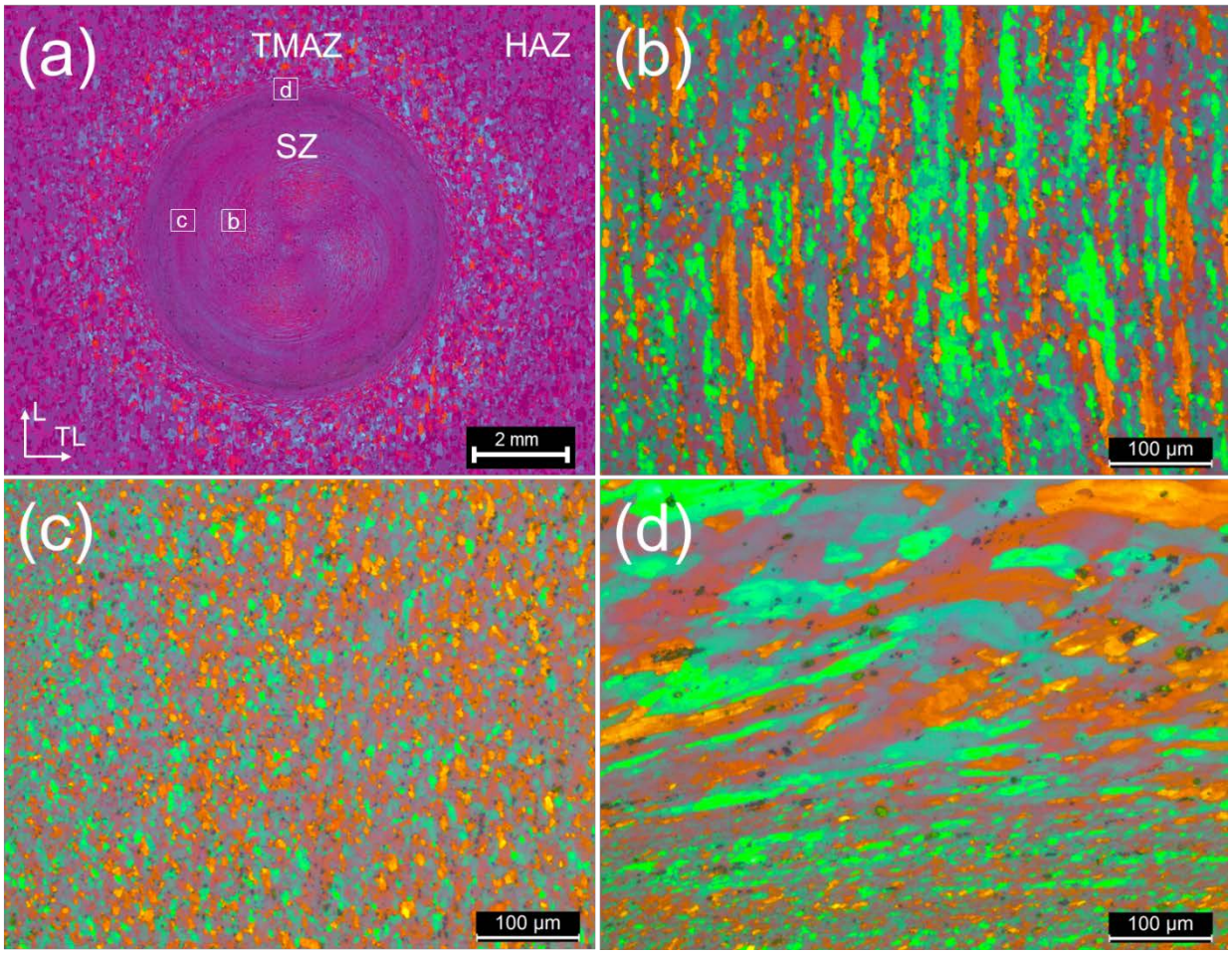

Figure 8 Microstructures in the L-TL plane section of keyhole closure welds: (a) Low magnification overview of RFSSW keyhole closure, (b) elongated grains in the SZ in the peripheral direction, (c) equiaxed grains in the SZ, (d) elongated grains in the TMAZ in peripheral direction

3.2.2 Microstructure formation

The stop-action technique was used to reveal the formation of microstructural features during the welding process. Figure 9(a) shows the cross-section after the stop-action technique was applied during the sleeve plunging phase. It is apparent that the material pushed away by the downward moving sleeve is located in the cavity underneath the retracting probe. The material from inside the tool was torn off due to application of the stop-action technique.

The material underneath the rotating sleeve is pressed into the center of the tool. The zone influenced by the sleeve is quite narrow. Because the base metal does not recrystallize evenly with the sleeve plunge depth, the recrystallization and material flow process is more complex. In the initial step of the process, when both of the rotating tool parts come in contact with the surface of the plug and workpiece, a zone of recrystallized material forms close to the surface of the plate. This recrystallized zone is approximately 0.6 mm deep in the weld center. In Figure 9(a), this zone is visible in the upper area of the material underneath the probe.

During sleeve plunge, the material that is not in direct contact with the sleeve is not inevitably recrystallized, as apparent especially in the center of the weld. The elongated grain structure from the plug base metal is still visible. The strain rates are assumed to be lower in the center of the weld where the material primarily moves upward during the sleeve plunge phase.

The material in the probe cavity is assumed to not rotate during the sleeve plunge phase. If it rotated, a zone of high shear rates would form in the lower areas of the probe cavity (approximately where the material was torn off in the stop-action experiments) because the plug material underneath the sleeve is not rotating. This process would force the material that is pushed into the probe cavity to pass this zone of high shear. Consequently, the material in the probe cavity would be recrystallized or highly deformed in the rotational direction.

The interface between the plug and surrounding workpiece is not broken into pieces and stirred during the sleeve plunging process, and in fact, it is pressed into the probe cavity. This interface is still visible but shows damage at higher magnification because of elongation due to the difference in travel between the sleeve and probe. The probe must retract to higher than the sleeve plunge depth to accommodate the same volume of displaced material. The parts of the interface directly underneath the sleeve are bent toward the center of the weld, indicating the material flow direction.

Figure 9(b) shows a cross-section in which the stop-action technique is applied during the sleeve retraction phase. In this scenario, the material from inside the tool cavity was torn off due to the sudden stop-action technique. The lower portion of the torn-off stub exhibits larger equiaxed grains. The rupture introduced additional plastic deformation into the stub. After the stop-action process, the stub remained in contact with

the tool for several minutes, maintaining the elevated temperature and thus enabling grain growth. The flaky surface appearance on the stub can be attributed to sleeve retraction during the stop-action process.

During the sleeve retraction phase, the probe pushes the material in the tool cavity downward, where high pressure forces the material laterally and slightly upward to fill the cavity left by the retracting sleeve. The material trapped inside the tool cavity shows much smaller grains than during the sleeve plunge phase, indicating recrystallization. Certain bands of lower grain size are visible, indicating high shear concavely in this material, similar to the final microstructure. Therefore, the rotation of the cylinder-like material is assumed to occur in layers. The areas of highest shear rate form the bands of smaller grain size. The band of un-recrystallized material in the center of the final weld is already separated inside the tool cavity. The cross-section in Figure 9(b) shows those leftover BM grains as highly distorted in the rotational direction in the weld center, which is caused by a higher distance of the cross-section to the exact center of the weld, as shown in Figure 9(a).

The initial interface between the plug and surrounding workpiece is stirred into the surrounding volume during this process stage. In the material trapped inside the tool cavity, remnants from the joining interfaces are only partially visible. After passing what is assumed to be the area of highest shear rates in the transition zone from inside the tool cavity to the final microstructure, the interface is no longer visible.

The material underneath the sleeve is bent in the direction of the weld center during plunge and has not been broken up during this phase. Because the sleeve must comply with a safety clearance to the backing, a portion of the interface at the lower end of the plug remains underneath the sleeve without becoming entirely shifted into the probe cavity. In contrast to the material that is redistributed from the cavity underneath the probe during the sleeve retraction phase, this material experiences only insufficient stirring. A possible weak point is formed that can initiate mechanical failure when loaded, as discussed in Chapter 3.3.2.

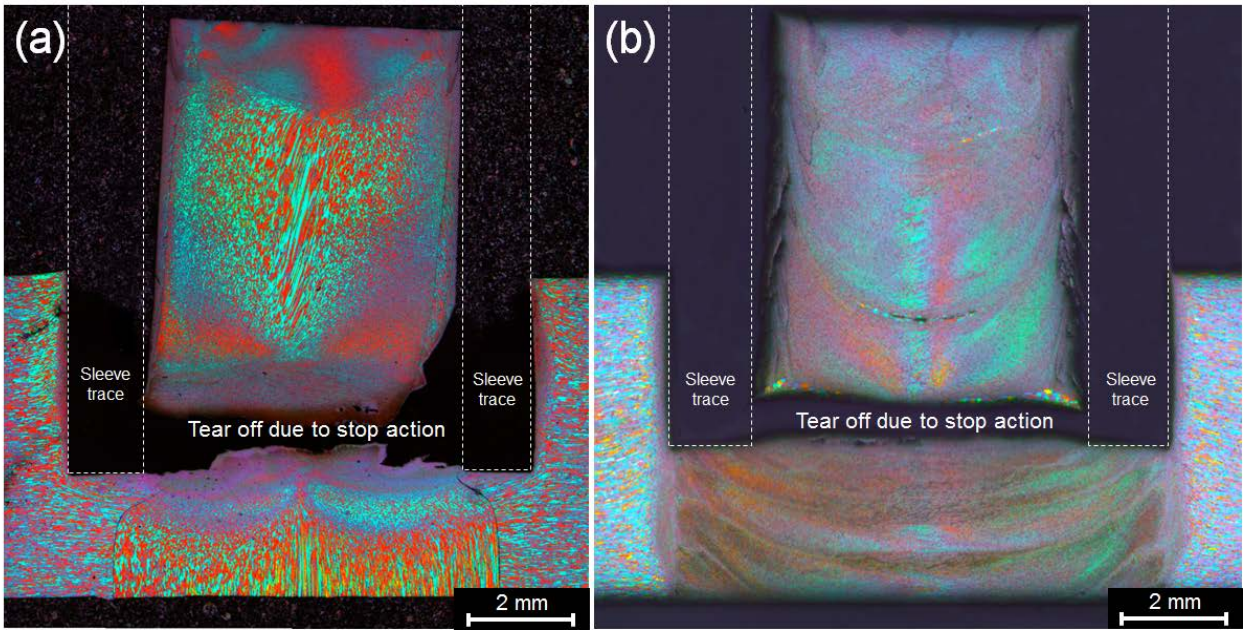

Figure 9 Low-magnification overview of stop-action sample: (a) during sleeve plunge, (b) during the sleeve retraction phase of the RFSSW keyhole closure weld

Figure 10 shows a stop-action sample during sleeve plunge with the sleeve still attached, explaining the behavior of material in direct contact with the rotating sleeve. The TMAZ shows upward deformation as well as downward deformation in regions close to the edge of the sleeve. The material up to approximately 200 µm recrystallizes underneath and on the sides of the rotating sleeve. Thus, the area of the SZ surrounding the sleeve forms during the sleeve plunge phase, and in the second half of the process, the material from inside the tool cavity is distributed against the prior recrystallized material.

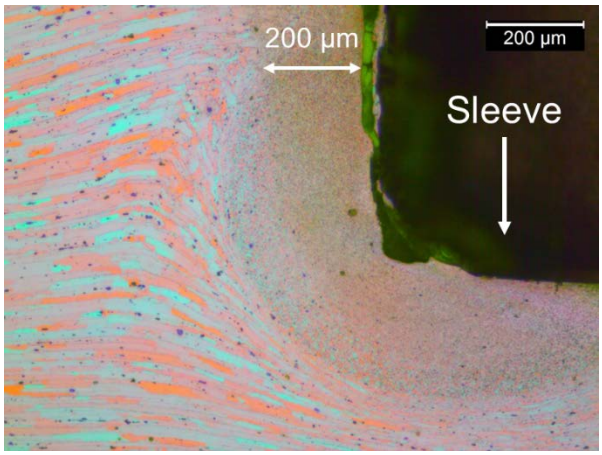

Figure 10 High magnification of the sleeve outer edge during sleeve plunge obtained via stop-action experiments

The discussed phenomena of microstructure formation explain why partial recrystallization is observed in keyhole closure welds. It is assumed that the high plunge depth/sheet thickness causes these phenomena because most of the shear required for recrystallization originates from direct contact of the BM with the rotating tool parts. At higher plunge depth, the material in the lower parts of the weld center neither come into contact with rotating tool parts nor are sheared inside the tool cavity during the process. The main directions of material flow in this area are upward during the sleeve plunge phase and downward during the sleeve retraction, which does not introduce sufficient deformation to begin recrystallization.

3.3 Mechanical properties

3.3.1 Microhardness

The microhardness distribution along the cross-section at mid-height at different post-weld natural aging times is presented in Figure 11. The keyhole closure welds formed using RFSSW develop a W-shape hardness distribution, which is typically observed for friction-based welding processes in precipitation-hardened aluminum alloys. The SZ shows a relatively constant hardness. With the beginning of the TMAZ, the hardness values decrease continuously to a minimum in the HAZ. From that point in the HAZ, with further distance from the center of the weld, the hardness values increase to the BM hardness. The hardness profile reveals a low-strength region in the HAZ that was not visible in microstructural analysis.

In the as-welded condition, the hardness in the SZ is approximately 36 % lower than the BM values, and the lowest hardness located in the HAZ is 42 % lower than the BM values. During post-weld natural aging, the hardness increases in all weld zones to 148 $HV_{0.2}$ in the SZ and 129 $HV_{0.2}$ in the areas of lowest hardness. These values are 20 % and 30 % below the BM values, respectively. After 4 weeks of post-weld natural aging, no further changes in hardness can be measured. After post-weld natural aging, the hardness profiles are in accordance with the findings of Shen et al. (2013) in overlap welds of AA 7075 using RFSSW. Additionally, the fully aged SZ hardness is in accordance with the SZ hardness found in the FSSW of AA 7075 and is similar to the hardness values in the AA 7075 sheet, which was solution heat treated and aged at room temperature for 7 days (149 HV) by Gerlich et al. (2006).

After aging, the lowest hardness is located approximately 10 mm on average from the center of the weld. The heating and thermal transients shown in the thermal cycle at 9 mm from the center of the weld in Figure 3 therefore generally represent the most unfavorable case for the base metal. The constant hardness in the SZ leads to the assumption that the temperature distribution is homogeneous in the SZ during welding.

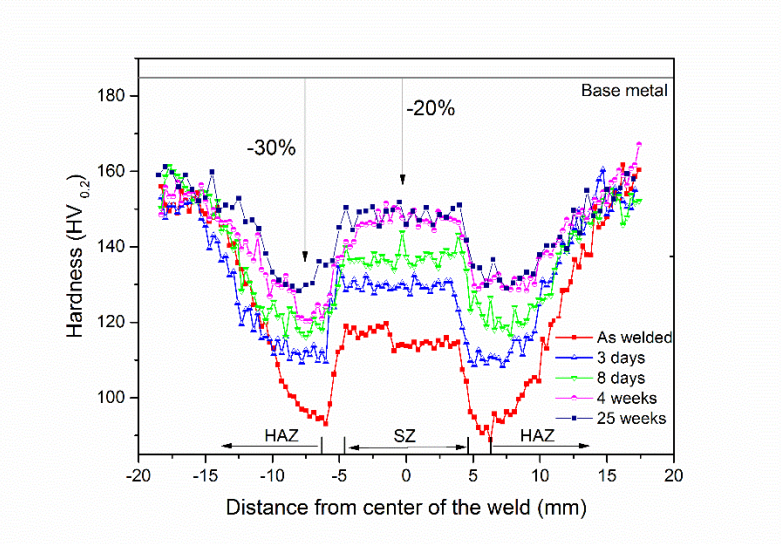

Figure 11 Hardness profile of the RFSSW keyhole closure weld at different post-weld natural aging durations welded at 1800 rpm and 0.85 mm/s

No influence of the process parameters on the absolute values of microhardness could be observed. Inside the tested process parameter window, the standard deviation of the average hardness in the SZ is 3.04 %, and it is 6.61 % for the measurements of lowest hardness. The higher value for lowest hardness measurements is due to the manner in which microhardness is measured. The hardness indentations are placed at a certain distance from each other, and one does not necessarily hit the exact position of lowest hardness, which increases the standard deviation of that measurement. Still, the distance of the lowest hardness shows a trend toward increase with increasing revolutions per mm during the welding. The higher heat input and increasing temperatures in the HAZ shift the thermal cycle that is most unfavorable for the BM to locations further away from the center of the weld. Similar results are indicated in the work of Pieta et al. (2014) in RFSSW of AA 2198-T8 sheets.

3.3.2 Analysis of tensile characteristics

Representative stress-strain curves and characteristic failure modes of keyhole closure welds using RFSSW are presented in Figure 12. The base metal results are in accordance with the literature data. The welded spots display a characteristic behavior under monotonic uniaxial loading showing two fracture modes. Failure mode 1 fractures in the HAZ in the region of lowest hardness, whereas failure mode 2 fractures in the outer regions of the SZ. Approximately 70 % of the tested samples failed with mode 2 fracture, and the fracture modes were not dependent on the process parameter. Welded samples begin to yield at 291 MPa (55 % of BM YS), whereas the ultimate tensile strength depends on the fracture mode. Samples with fracture mode 1 show an ultimate tensile strength (UTS) of 425 MPa (74 % of BM UTS), and samples with fracture mode 2 fail earlier, at 401 MPa (70 % of BM UTS). With a standard deviation of 5.1 %, the yield strength

showed no dependence on the welding parameters. Similarly, the process parameters did not influence the ultimate tensile strength significantly. The standard deviation of the ultimate tensile strength was 1.4 % for mode 1 failure and 5.2 % for mode 2 failure.

The two failure modes show the main weakened areas in the keyhole closure welded samples. The first example is the area of lowest strength in the HAZ introduced by the thermal cycle during welding. This weakened zone can be observed in the microhardness distribution, and no changes in microstructural features can be observed. The second example is the outer regions of the SZ and cannot be identified in microhardness or microstructure analysis.

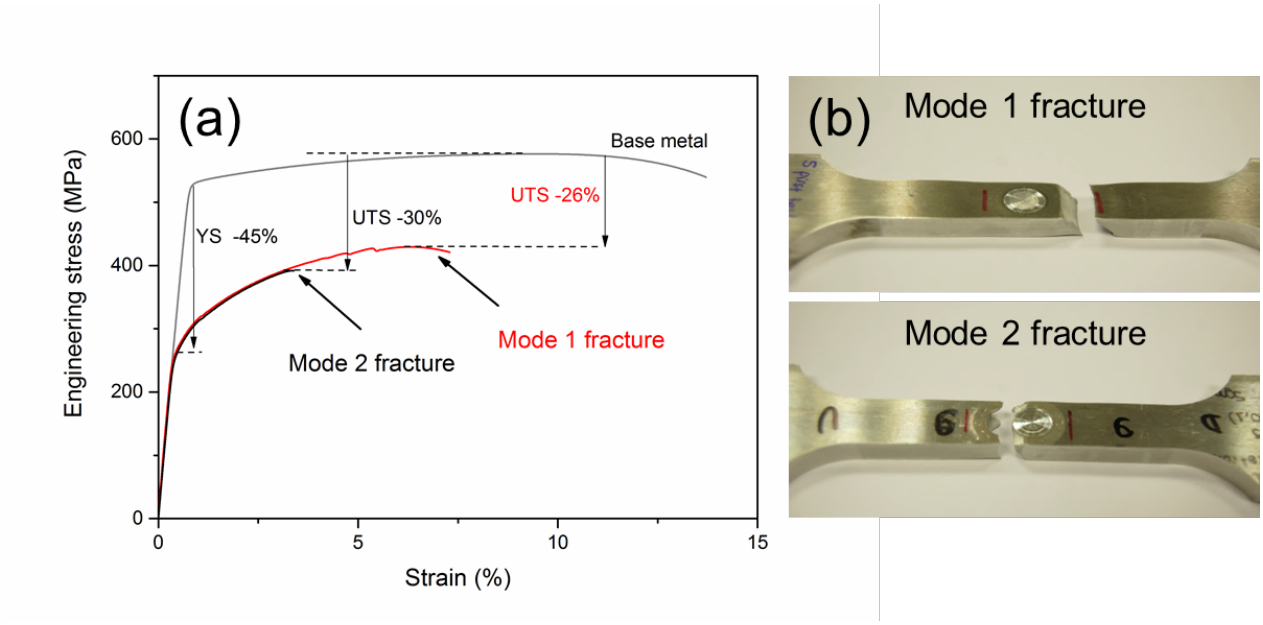

Figure 12 TT characteristics of keyhole closure welds: (a) stress-strain diagram showing typical curves and (b) characteristic fracture modes with failure in the HAZ (mode 1) and in the SZ (mode 2)

Mode 1 fracture shows typical microvoid coalescence fracture with transgranular and intergranular fractions and 45° degree fracture. The fracture surface shown in Figure 13(a) exhibits large 10-50 µm diameter dimples nucleated at large second-phase particles as well as broad intergranular fractions originated from the shear along the grain boundaries of the large pancake-shaped grains. At higher magnification, Figure 13(A) displays additional small dimples indicating fracture at fine dispersion phases in a typical slip plane.

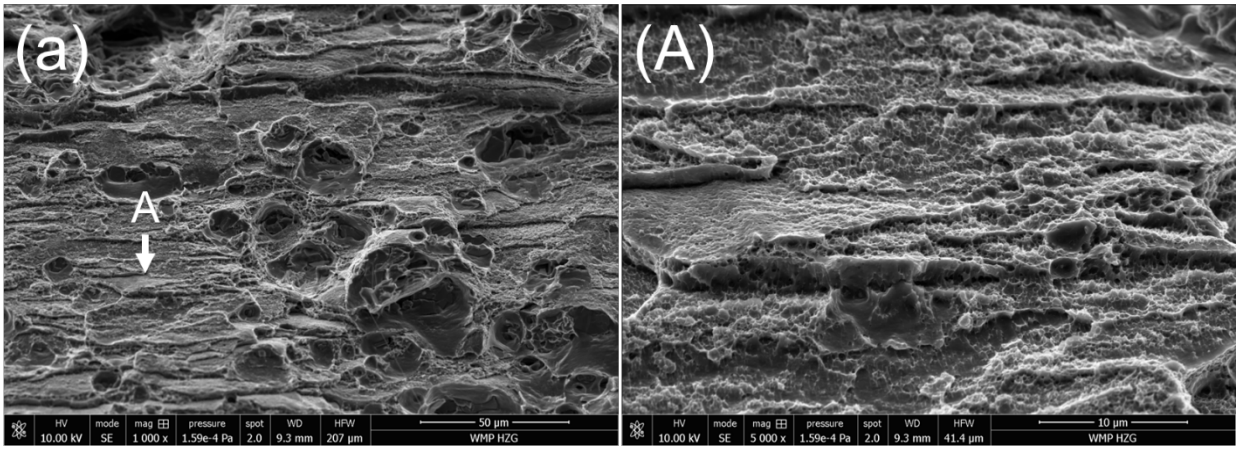

Figure 13 Scanning electron micrographs of a) mode 1 fracture type from the center of the fracture surface and A) magnified view of region A marked in (a)

Scanning electron macrographs of the overall fracture mode 2 is presented in Figure 14(a) and higher magnification views of the regions marked A, B and C in Figure 14(a) are shown in Figure 14(A), (B) and (C), respectively. Additionally, higher magnifications of the marked regions in Figure 14(A) and (B) are shown in Figure 14(A_1), (A_2), (B_1) and (B_2). The fracture initiates at a weak bonded area in the initial interface between the plug and surrounding workpiece in the undermost region of the welded plate, as shown in Figure 14(A). Figure 14(A_1) shows small dimples indicating low plastic deformation. From this point, the crack propagates upward, passing the region shown in Figure 14(A_2) with larger and deeper dimple features, which indicate that plasticity increases and the metallurgy combination becomes preferable. Subsequently, the crack propagates upward with a tendency outward, away from the center of the weld. As the crack passes the welded interface described in Chapter 3.2.2, inhomogeneity appears, as shown in Figure 14(B). The region shown in Figure 14(B_1) is characterized by a flat fracture surface with shallow and equiaxed dimples indicating a low deformation level and is assumed to originate from weak bonding in the welded interface. However, what is assumed to be the transition zone from the welded interface to the outer regions of the SZ in Figure 14(B_2) shows certain intergranular fracture shares with small dimples on the surface of the SZ grains. In the upper sections of the fracture surface, the crack follows a more outward-bending angle and ends in the interface between the SZ and TMAZ on the surface of the welded plate. Figure 14(C) shows a fracture surface with a combination of shallow dimples and tearing edges as the crack propagates into the TMAZ, with the fracture path indicating larger, in the rotational direction elongated grains, as shown in Figure 8(d).

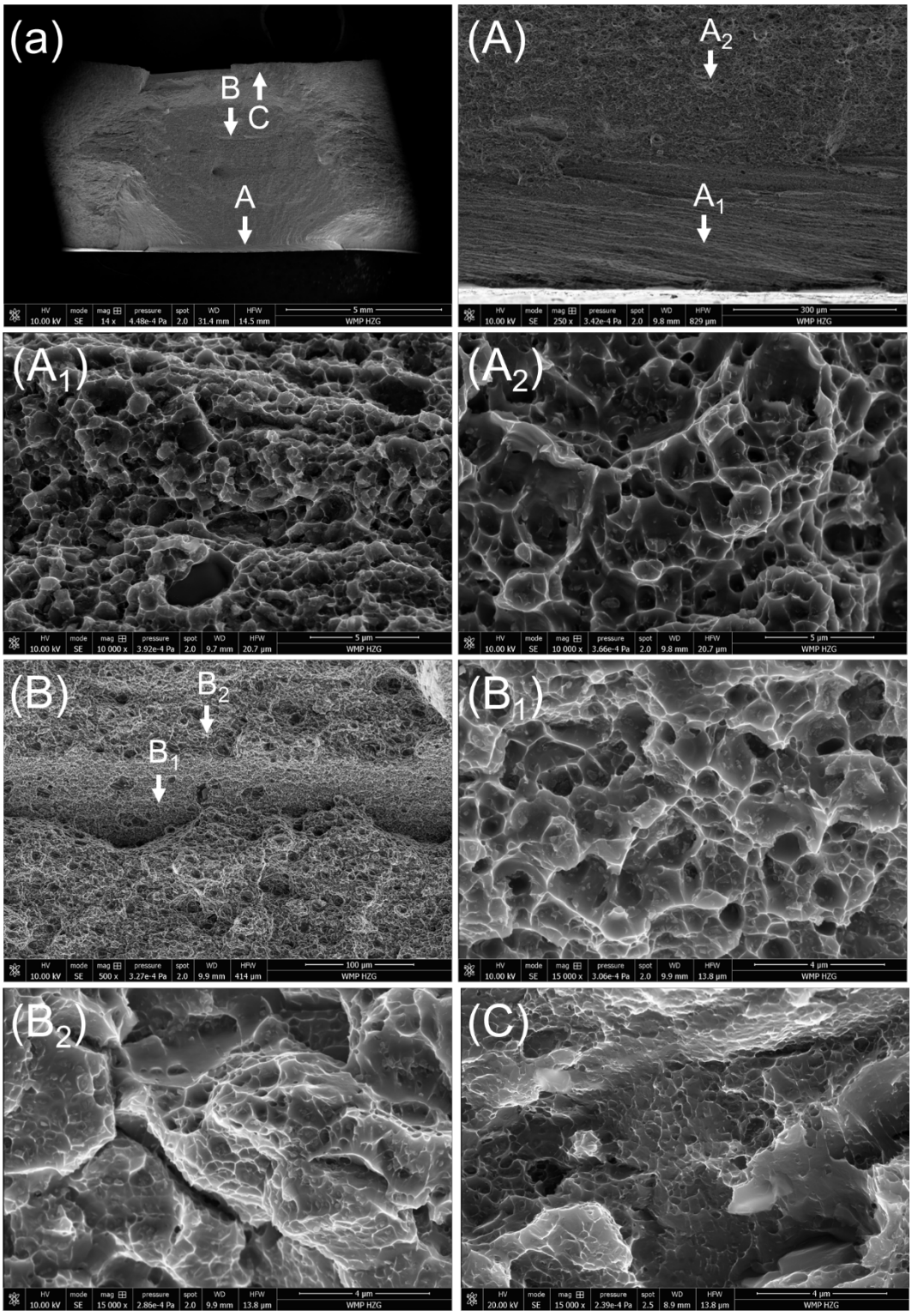

Figure 14 Scanning electron micrographs of a) mode 2 fracture type; A), B) and C) magnified views of regions A, B and C marked in (a); (A_1) and (A_2) magnified views of regions A_1 and A_2 in (A), and (B_1) and (B_2) magnified views of regions B_1 and B_2 in (B)

Strain maps and the strain distribution at the vertical centerline through the center of the weld acquired via DIC are presented in Figure 15. During tensile testing, strain concentrates near 20 mm around the center of the weld, which corresponds to the HAZ dimensions, resulting in a lower total elongation compared with the BM values. Yielding begins in the areas of lowest hardness in the HAZ, as shown in Figure 15(a). At higher stress, most of the strain accumulates in the areas of low strength in the HAZ at approximately 10 mm from the center of the weld. Additionally, strain concentration peaks in the outer regions of the SZ indicate the upcoming failure mode 2. The strain distribution is inversely proportional to the hardness distribution reported in Figure 11 except for those peaks that become apparent due to the high resolution of the DIC measurement.

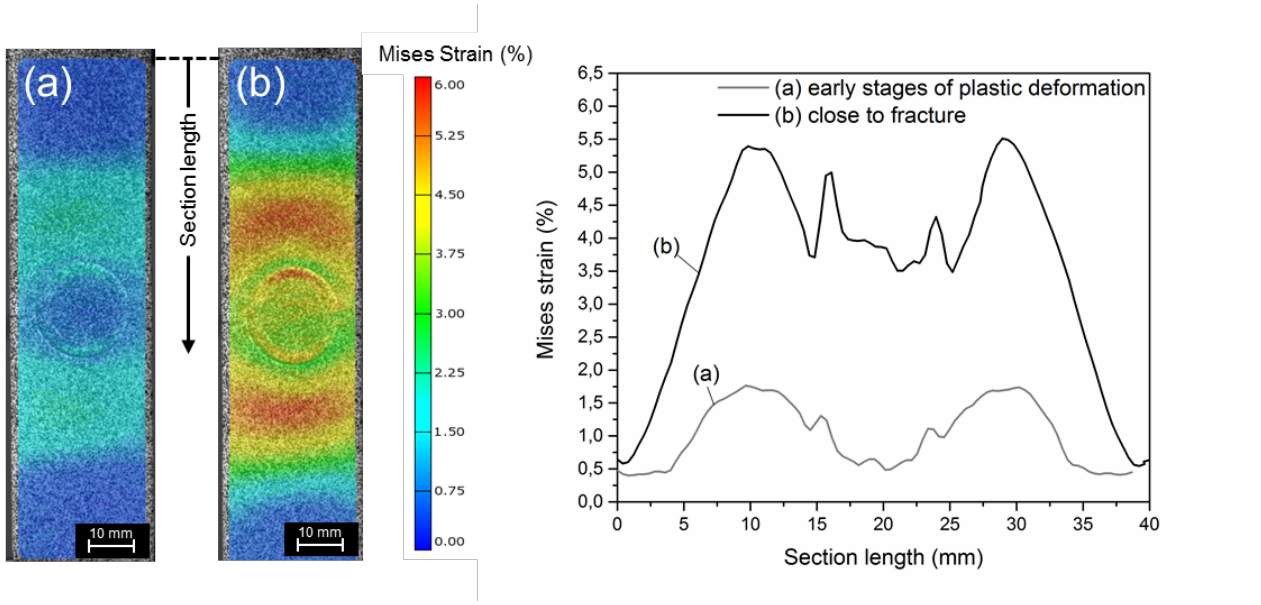

Figure 15 Strain maps and strain distribution through the centerline of the tested coupons during tensile testing of keyhole closure welded samples (a) at early stages of plastic deformation and (b) close to fracture

The yield strength increases significantly during post-weld natural aging, as shown in Figure 16. The increase in yield strength correlates with the increase of the hardness in the area of lowest strength in the HAZ because this is the region where yielding begins. Similar to the findings from microhardness analysis, after 4 weeks of post-weld natural aging, no further changes in mechanical properties can be measured.

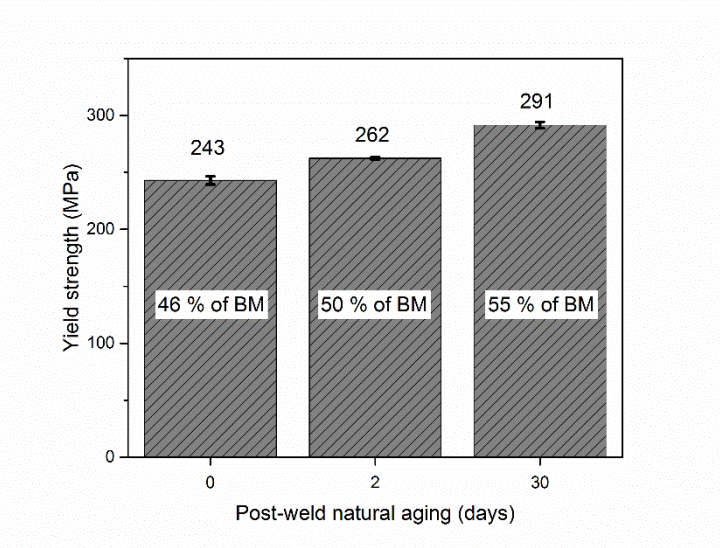

Figure 16 Effect of post-weld natural aging on the yield strength of keyhole closure welded samples using RFSSW

Application of dwell time during welding decreases the mechanical properties of the welds. The influence of dwell time on the yield strength in fully post-weld aged samples is shown in Figure 17. Additional dwell time increases the energy input during welding, and therefore, the temperature exposure in the HAZ increases, which in turn decreases the strength. Therefore, because flawless welds are achievable without dwell time, it is not recommended to use dwell time for keyhole closure welding of AA 7075-T6 using RFSSW.

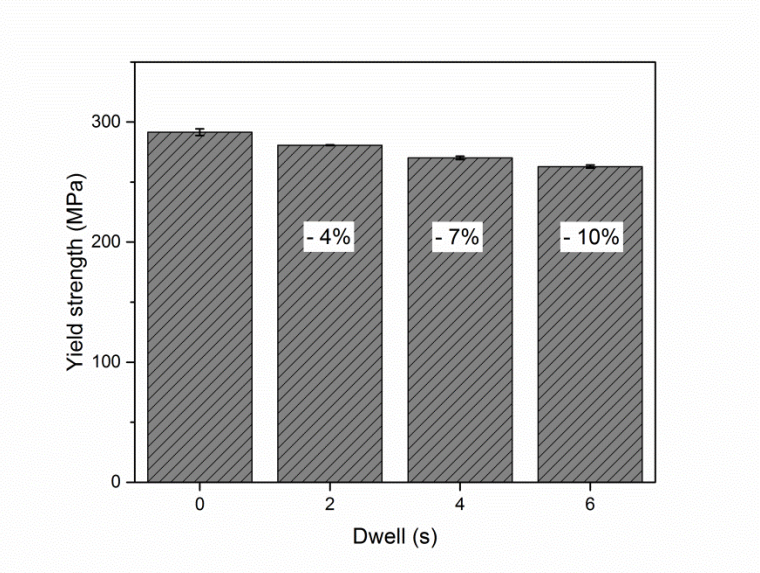

Figure 17 Influence of dwell time on the yield strength of keyhole closure welded samples

4 Conclusions

This work investigated the thermal cycle, microstructure and mechanical properties of keyhole repair welds in AA 7075-T651 performed via refill friction stir spot welding. The analysis produced the following observations:

1. Keyhole closure welds were achieved in 6 mm plates of high-strength AA 7075-T651 using RFSSW, producing defect-free and highly efficient welds.
2. Post-weld natural aging was shown to be highly significant for the mechanical properties of the welds. During aging, the strength increases from 58 % to 70 % of the BM hardness in the area of lowest hardness in the HAZ and from 46 % to 55 % of the BM YS. Post-weld natural aging stabilized after 4 weeks. Dwell time was shown to decrease the weld strength as YS is reduced by 10 % when 6 seconds of dwell time are applied during the welding process.
3. The sealed through-hole welds show a typical W-shaped hardness distribution with hardness values of 80 % and 70 % of the BM values in the SZ and regions of lowest hardness in the HAZ, respectively. Analysis of the tensile characteristics revealed a YS that is 55 % of the BM values with plastic deformation beginning in the HAZ. Two fracture modes were observed. Mode 1 fracture failed in the HAZ with an UTS that is 74 % of the BM strength, and fracture mode 2 failed in the SZ with 70 % of the BM strength. Fracture mode 1 fails in typical ductile fracture at a 45° angle. For mode 2 failure, the crack initiates in the lowest portions of the SZ at the weak-bonded plug-workpiece interface remnant, and from there, it passes upward and slightly outward through the SZ to end in the transition zone from the SZ to the TMAZ on the surface of the welded plate.
4. The thermal cycle shows typical high heating rates during the sleeve-plunge phase with peak temperatures reaching 540°C in the center of the weld. The supplied energy shows a linear correlation with the revolutions per mm plunge/retract indicating consistent friction condition. An increase in energy input and peak temperatures in the HAZ could be determined as the revolutions per mm plunge/retract increase, but the absolute values of mechanical properties, such as YS, UTA and hardness, did not change significantly. The increased energy input is assumed to shift the position of highest strength loss in the HAZ further away from the center of the weld.
5. Microstructure analysis reveals flawless welds with typical microstructural zones. Using the stop-action technique, partial recrystallization was observed in the SZ for the first time. Partial recrystallization occurs in the center of the welds and is believed to be caused by the high plunge depth.

5 References

Behmand, S., Mirsalehi, S., Omidvar, H., Safarkhanian, M., 2015. Filling exit holes of friction stir welding lap joints using consumable pin tools. Science and Technology of Welding and Joining 20, 330-336.

Çam, G., Mistikoglu, S., 2014. Recent Developments in Friction Stir Welding of Al-alloys. J Mater Eng Perform 23, 1936-1953.

Du, B., Sun, Z., Yang, X., Cui, L., Song, J., Zhang, Z., 2016. Characteristics of friction plug welding to 10 mm thick AA2219-T87 sheet: Weld formation, microstructure and mechanical property. Materials Science and Engineering A 654, 21-29.

Dunkerton, S., Nicholas, D., Sketchley, P., 1991. Repairing defective metal workpiece–by friction welding with a metal plug, In: TWI (Ed.), Great Britain Patent Application.

Gerlich, A., Avramovic-Cingara, G., North, T.H., 2006. Stir zone microstructure and strain rate during Al 7075-T6 friction stir spot welding. Metallurgical and Materials Transactions a-Physical Metallurgy and Materials Science 37A, 2773-2786.

Han, B., Huang, Y.X., Lv, S.X., Wan, L., Feng, J.C., Fu, G.S., 2013. AA7075 bit for repairing AA2219 keyhole by filling friction stir welding. Materials & Design 51, 25-33.

Huang, Y., Han, B., Tian, Y., Liu, H., Lv, S., Feng, J., Leng, J., Li, Y., 2011. New technique of filling friction stir welding. Science and Technology of Welding and Joining 16, 497-501.

Ji, S., Meng, X., Zeng, Y., Ma, L., Gao, S., 2016a. New technique for eliminating keyhole by active-passive filling friction stir repairing. Materials & Design 97, 175-182.

Ji, S.D., Meng, X.C., Huang, R.F., Ma, L., Gao, S.S., 2016b. Microstructures and mechanical properties of 7N01-T4 aluminum alloy joints by active-passive filling friction stir repairing. Materials Science and Engineering: A 664, 94-102.

Lloyd, D.J., Chaturvedi, M.C., 1982. A calorimetric study of aluminium alloy AA-7075. Journal of Materials Science 17, 1819-1824.

Metz, D.F., Barkey, M.E., 2012. Fatigue behavior of friction plug welds in 2195 Al–Li alloy. International Journal of Fatigue 43, 178-187.

Metz, D.F., Weishaupt, E.R., Barkey, M.E., Fairbee, B.S., 2012. A Microstructure and Microhardness Characterization of a Friction Plug Weld in Friction Stir Welded 2195 Al-Li. Journal of Engineering Materials and Technology 134, 021005.

Pieta, G., dos Santos, J., Strohaecker, T.R., Clarke, T., 2014. Optimization of Friction Spot Welding Process Parameters for AA2198-T8 Sheets. Materials and Manufacturing Processes 29, 934-940.

Reimann, M., Gartner, T., Suhuddin, U., Göbel, J., dos Santos, J.F., 2016. Keyhole closure using friction spot welding in aluminum alloy 6061–T6. Journal of Materials Processing Technology 237, 12-18.

Reimann, M., Goebel, J., Gartner, T.M., dos Santos, J.F., 2017. Refilling termination hole in AA 2198-T851 by refill friction stir spot welding. Journal of Materials Processing Technology 245, 157-166.

Shen, Z., Yang, X., Zhang, Z., Cui, L., Li, T., 2013. Microstructure and failure mechanisms of refill friction stir spot welded 7075-T6 aluminum alloy joints. Materials & Design 44, 476-486.

Totten, G.E., MacKenzie, D.S., 2003. Handbook of Aluminum: Vol. 1: Physical Metallurgy and Processes. Marcel Dekker, Inc., New York, NY, USA.

Zhang, G.F., Jiao, W.M., Zhang, J.X., 2014. Filling friction stir weld keyhole using pin free tool and T shaped filler bit. Science and Technology of Welding and Joining 19, 98-104.

Zhao, Y., Liu, H., Yang, T., Lin, Z., Hu, Y., 2015. Study of temperature and material flow during friction spot welding of 7B04-T74 aluminum alloy. Int J Adv Manuf Technol, 1-9.

Zhao, Y.Q., Liu, H.J., Chen, S.X., Lin, Z., Hou, J.C., 2014. Effects of sleeve plunge depth on microstructures and mechanical properties of friction spot welded alclad 7B04-T74 aluminum alloy. Materials & Design 62, 40-46.
Zhou, L., Liu, D., Nakata, K., Tsumura, T., Fujii, H., Ikeuchi, K., Michishita, Y., Fujiya, Y., Morimoto, M., 2012. New technique of self-refilling friction stir welding to repair keyhole. Science and Technology of Welding and Joining 17, 649-655.